ACERP: Vol. 6, No.2, (Spring 2020) 7-16

Advanced Ceramics Progress

Research Article

Journal Homepage: www.acerp.ir

Investigating the Abrasive Wear Resistance of Thermal-Sprayed WC-Based Coatings

S. M. Nahvi [a] *

[a] *Department of Materials Engineering, Isfahan University of Technology, Isfahan 84156-83111, Iran*

PAPER INFO

Paper history:

Received 1 April 2020
Accepted in revised form 13 April 2020

Keywords:

Abrasive Wear
WC–FeCrAl
WC–NiMoCrFeCo
HVOF

ABSTRACT

The purpose of this research was to investigate the abrasive wear behavior of WC–NiMoCrFeCo (WC-N) and WC–FeCrAl (WC-F) coatings deposited by high-velocity oxygen fuel (HVOF) spraying. The abrasive wear resistance was evaluated by a dry sand rubber wheel (DSRW) test rig using abrasives silica 70 and alumina 60, and the values were then compared to those of conventional WC-Co (WC-C) coatings. The abrasive wear with silica 70 indicated the "soft abrasion" regime, while alumina 60 abrasive caused a "hard abrasion" for all coatings. Moreover, the wear rate of the coatings abraded by alumina 60 was around 1.2-7.8 times greater than that of silica 70. WC-F exhibited the greatest wear resistance compared to other coatings tested by silica 70 due to its lower mean free path and higher hardness compared to other coatings. WC-C coating revealed the cobalt matrix removal followed by WC fracture and pullout using abrasive silica 70, while WC-F and WC-N coatings represented a combination of subsurface cracking, WC pullout, and fracture. Abraded by alumina 60, WC-C, WC-F, and WC-N coatings showed the evidence of grooving, pitting, and cutting. Moreover, WC-C coating had the highest wear resistance due to its high fracture toughness and low porosity, protecting WC-C coating against severe cracking and grooving, respectively. Cross-sectional images of the wear scars revealed a significant sub-surface cracking for WC-F and WC-N coatings while no significant cracking could be detected for WC-C coating.

1. INTRODUCTION

The superior composite structure of WC-Co thermal spray coatings includes a hard ceramic phase (WC) and a ductile metallic binder (Co). This structure provides an exceptional combination of high hardness, fracture toughness, and wear resistance, which makes them useful in a broad range of industrial applications such as seat and gate components in petroleum, pinch rolls, and bridle rolls in steel rolling, and aircraft landing gear in aerospace industries [1-5].

Among the common thermal spray techniques for WC-Co coatings deposition including air plasma spraying (APS), detonation spray coating (DSC), and high-velocity oxygen-fuel (HVOF) spraying, the latter provides higher velocity and lower temperature for in-flight particles and produces more compacted coatings with sustaining a larger fraction of retained WC phase [4]. In addition, HVOF-sprayed WC-Co coatings are considered as a viable alternative to hard chromium plating owing to their superior wear resistance and more environmentally friendly properties [5,6]. Nevertheless, the major concern in HVOF-sprayed WC-Co coatings is to control WC decarburization during the spraying process to avoid the formation of brittle phases, such as W_2C, metallic W, and nano-crystalline Co-W-C [7-9]. Numerous strategies have been implemented to control WC decarburization via the optimization of spray parameters [10-13], tailoring the composition of WC-Co powder [14,15], and utilizing metal-clad WC-Co powders [4,6,16,17]. The optimum wear resistance of WC-Co coatings is achievable in a microstructure including minimum WC decarburized and maximum retained WC particles distributed within the metallic cobalt matrix [18-21].

The abrasive wear resistance is one of the most important factors affecting the tribological performance of WC-based cermet coatings in a variety of practical conditions. For instance, the WC-Co coated cylinder rod

* Corresponding Author Email: mehran.nahvi@cc.iut.ac.ir (S. M. Nahvi)

https://doi.org/10.30501/acp.2020.107466

of landing gear is exposed to impact and adherence of sands and other hard particles imposing crucial damage to the coatings' surface during landing and ground operation of aircraft [5]. Previous works have mostly focused on the effect of WC carbide grain size on the abrasive wear behavior of HVOF-sprayed WC-Co coatings. For example, Stewart et al. [22] and Dent et al. [23] reported inferior abrasive wear resistance for nanostructured WC-Co compared to the conventional coarse-grained coatings due to the extensive dissolution and decarburization of nano-sized WC grains during HVOF spraying. In contrast, Saha et al. [24] and Baik et al. [17] reported an opposite trend for nanostructured WC-Co coatings deposited from Co-coated WC-Co powder. This behavior was attributed to the presence of the protective Co layer around individual nanostructured WC-Co powder particles, which reduces the interactions between HVOF flame and WC particles, and thereby, lowers the extent of decarburization [17,24].

The purpose of the present study was to evaluate the soft and hard abrasive behavior of the WC-based cermet HVOF sprayed coatings with complicated alloyed binders, i.e. WC–NiMoCrFeCo and WC–FeCrAl, using a dry sand rubber wheel testing and compare the outcomes of examinations with conventional WC-Co coatings. The microstructural and mechanical properties of these coatings have been studied in detail, and presented elsewhere [7].

2. EXPERIMENTAL PROCEDURES

2.1. THERMAL SPRAY PROCESS

Three different powders including WC-NiMoCrFeCo (WC-N), WC-FeCrAl (WC-F), and WC-Co (WC-C) were utilized as HVOF feedstock materials. All powders were agglomerated and sintered spheroids with the nominal diameters in the range of 15-45µm. WC grain size and chemical composition of the powders are presented in Table. 1.

TABLE 1. WC grain size and chemical composition of feedstock powders

Powder	Company	WC size (µm)	Composition (wt%)								
			W	Ni	Mo	Cr	Fe	Co	Al	C	O
WC-C (83-17%wt)	Sulzer Metco	1.0	77.98	-	-	-	0.04	16.82	-	5.16	-
WC-F (85-15%wt)	H.C. Starck	0.5	79.05	-	-	3.40	10.79	-	1.02	5.58	0.16
WC-N (85-15%wt)	H.C. Starck	0.7	79.97	8.47	2.24	2.15	0.84	0.62	-	5.65	0.06

Plain-carbon steel (0.12%C, 0.7%Mn) sheets with the hardness of 246$HV_{0.3}$ and dimensions of 59×25×3mm^3 were used as substrate. The substrates were cleaned and grit blasted with ~250µm brown alumina to degrease and roughen the surface. The feedstock powders were sprayed onto the substrates using a Praxair/UTP Top-Gun HVOF spray system with parameters listed in Table 2. Hydrogen and nitrogen were employed as the fuel and carrier gases, respectively. The sprayed samples were cooled with compressed air jets, and collected at the end of the treatment for subsequent characterization.

TABLE 2. Spray parameters employed for coating depositions

Spray Parameter	WC-C	WC-F	WC-N
O_2 flow rate (l min^{-1})	240	240	240
Fuel gas (H_2) flow rate (l min^{-1})	640	640	640
Carrier gas (N_2) flow rate (l min^{-1})	17	17	17
Spray distance (mm)	250	250	250
Number of pass	40	40	51
Length of pass (mm)	77	77	76
Carousel diameter (mm)	280	280	280
Substrate velocity (m s^{-1})	1	1	1
Gun transverse speed (mm s^{-1})	5	5	5
Coating time (s)	674	729	924
Consumption of powder (g)	710	635	555
Coating thickness (µm)	445	436	260
Powder feed rate (g min^{-1})	63	52	36

2.2. Abrasive wear evaluation

The samples were examined using a dry sand rubber wheel test rig modified by Stevenson and Hutchings to evaluate the coatings' behavior under three-body low-stress abrasion conditions [25]. As illustrated in Fig. 1, the coating samples were held in a slot at the top of the rotating wheel to control the feed of abrasive to be passed between the wheel and the sample.

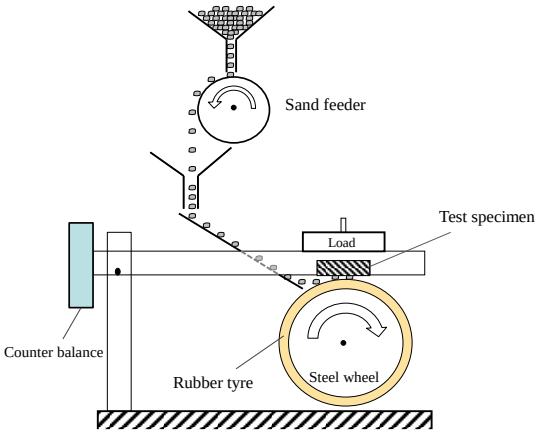

Figure 1. Schematic representation of dry sand rubber wheel abrasion test apparatus

The rubber wheel consisted of a cast polyurethane elastomer (monothane A60; CIL, Preston, UK) around an inner steel wheel with an overall diameter as much as 227mm. The tire had a width as much as 12mm and an international rubber hardness as much as 63±3 degrees as measured by a Wallace Hardness Meter. The rotation speed of the rubber was set at 195rpm, equivalent to a sliding speed of 2.32m.s^{-1}, according to ASTM standard G65 [26].

In this work, two types of abrasives were used:

1. Angular alumina 60 (Abrasive Developments, Henley-in-Arden, UK) with a size range as much as 212-300μm and sand feed rate of 2.64g.s^{-1};
2. Rounded silica 70 (The David Ball Company, Bar Hill, UK) with a size range as much as 180-250μm and sand feed rate of 2.37g.s^{-1} (Fig. 2).

The hardness of the abrasive particles was measured using a LECO M-400 microhardness tester with a 300gf load. The abrasive particles were mounted in a hot hardening resin and polished to preparation of a flat cross-section of the particles to indentation. The reported hardness value is the average value of 5 indents taken from different regions. The Vickers's hardness of silica 70 and alumina 60 abrasives measured on the polished cross-sections with a 300gf indentation load were 1138±47HV$_{0.3}$ and 2144±25HV$_{0.3}$, respectively.

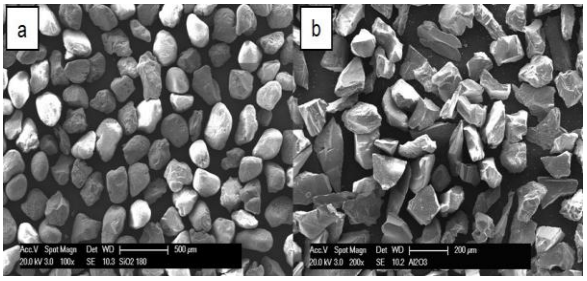

Figure 2. SEM micrograph of (a) silica 70 and (b) alumina 60 abrasive particles

In the wear behavior study, four different loadings of 19.6, 49, 98, and 127.5N were applied. The mass loss of the coatings was measured before and after each test using a GF-200 balance (A&D Instruments Ltd., Tokyo, Japan) with 10g capacity and 0.001g accuracy. Prior to the mass loss measurements, the coated samples were rinsed in methanol and dried. Abrasion distances of 800, 1600, 2400, 3200, and 4000 were considered for the coating samples. The wear rate was acquired from the gradient of the steady-state part of the mass loss versus sliding distance graph.

The worn surface of the coated samples was examined by an optical microscopy, scanning electron microscopy (Philips XL30, FEI Ltd, Cambridge, UK) with an accelerating voltage of 20kV in secondary electron (SE) and back-scattered electron (BSE) imaging modes to explore the wear mechanism of the coatings.

3. RESULTS

3.1. MICROSTRUCTURE AND MECHANICAL PROPERTIES

Detailed microstructural and mechanical properties of WC-C, WC-F, and WC-N coatings have already been reported [7]. Table 3 summarizes the most important microstructural and mechanical features of WC-C, WC-F, and WC-N coatings.

TABLE 3. Microstructural and mechanical properties of WC-C, WC-F, and WC-N coatings [7]

Coating	Carbide (vol%)	(W_2C/WC)	Carbon loss (%)	Porosity (vol %)	Microhardness ($HV_{0.3}$)	K_{IC} ($MPam^{1/2}$)
WC-C	55	9.14	30	1.8	1305 ± 71	5.9 ± 0.13
WC-F	58	12.48	16	5.1	1498 ± 82	3.1 ± 0.23
WC-N	59	40.42	36	2.2	1254 ± 38	2.8 ± 0.27

WC decarburization occurred during HVOF spraying of all materials designations. The minimum carbon loss was obtained for WC–F (16%), while WC–C and WC–N coatings experienced greater extents of decarburization of 30% and 36%, respectively. Cross-sectional SEM images exhibited a typical splat-like microstructure with dark and bright areas, which refers to the regions with lower, and higher mean atomic number, respectively. WC particles with angular morphology were observed in the darker areas of the matrix, indicating insignificant WC dissolution into the matrix. In the brighter regions, however, WC particles were observed with a more rounded morphology, which partially or fully enclosed by an irregular-shaped W_2C phase with brighter contrast [7].

The X-ray diffraction (XRD) analysis revealed that W_2C/WC peak ratio of WC–N (40.42%) is significantly higher than that of WC–F (12.48%) and WC–C (9.14%) coatings, indicating the highest level of W_2C phase formed in WC–N coating [7].

The WC–F coating showed the maximum micro-hardness (1498HV$_{0.3}$) compared to WC–C (1305HV$_{0.3}$) and WC–N (1254HV$_{0.3}$). The WC–N and WC–F coatings with almost identical volume fractions of carbide phases, comprising both the retained WC and newly precipitated W_2C (see Table 3), showed a significant difference in their hardness values. This can be explained by the lower carbon loss and W_2C/WC

ratio of WC–F coating leading to the higher fraction of retained WC phase in comparison to WC–N coating [7]. The cumulative distribution of the fracture toughness of the coatings revealed the higher fracture toughness of WC–C coating with the mean value of 5.9MPam$^{1/2}$ compared to WC–F and WC–N coatings with mean values of 3.1 and 2.8MPam$^{1/2}$, respectively [7].

3.2. ABRASIVE WEAR BEHAVIOR

3.2.1. ABRASIVE WEAR RATE

The abrasive wear rate of WC-C, WC-F, and WC-N coatings was determined using the least square fit method in the linear (steady-state) region. Steady-state wear rates of the coatings abraded by alumina 60 and silica 70 abrasives under the applied loads of 19.6, 49, 98, and 127.5 N are plotted in Fig. 3.

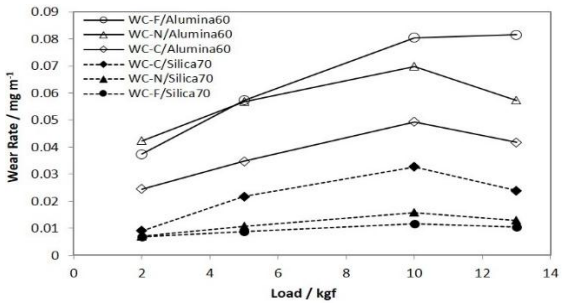

Figure 3. Variation of wear rate as a function of applied load for WC-C, WC-F, and WC-N coatings abraded by silica 70 and alumina 60

In all cases, the wear rate of the coatings abraded by alumina 60 is ~1.2-7.8 times higher than silica 70 abrasive. Hutchings et al. [27] reported that the wear rate is sensitive to the ratio of abrasive hardness (Ha) to the surface hardness (Hs); whereas, Ha/Hs>1.2 causes "hard abrasion" regime, while Ha/Hs<1.2 leads to "soft abrasion" one. Fig. 4 plots the Ha/Hs values for WC-C, WC-F, and WC-N coatings abraded by silica 70 and alumina 60. Obviously, the abrasive wear with alumina 60 is located in the "hard" abrasion region whereas silica 70 causes "soft" abrasion to all coatings. As for the coatings abraded by silica 70, WC-C showed the maximum wear rate of 0.0327mg.m^{-1} under 10kgf applied load, while the minimum wear rate in the range of 0.0069-0.0116mg.m^{-1} was obtained for WC-F coating.

The wear rate increased to the ranges of 0.0245-0.0493 and 0.0374-0.0698mg.m^{-1}, respectively in the case of WC-C and WC-N coatings abraded by alumina 60, with increasing the applied load from 2 to 10kgf. Further increase in the applied load to 13kgf resulted in the wear rate decline to 0.0417 and 0.0573mg.m^{-1} for WC-C and WC-N coatings, respectively. The wear rate of WC-F coating exhibits an upward trend from 0.0374 to 0.0804mg.m^{-1} with increasing the applied load from 2 to 10kg followed by a marginal increase to 0.0815mg.m^{-1} with further load rising to 13kgf.

Accordign to Fig. 3, it is obvious that the type of abrasive significantly affects the abrasive wear resistance of the coatings; e.g., WC-F and WC-C present the highest wear resistance for silica 70 and alumina 60, respectively.

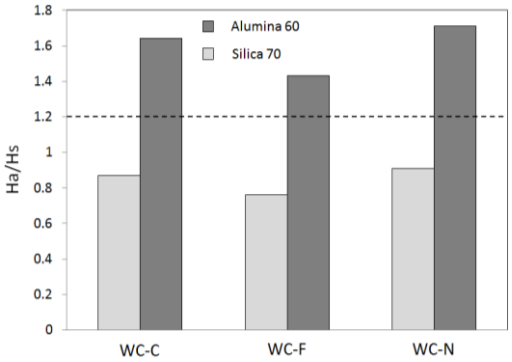

Figure 4. Plot showing transition between "hard" and "soft" abrasive wear mechanisms ($\frac{H_a}{H_s} = 1.2$) for the coatings abraded by silica 70 and alumina 60

3.2.2. WEAR SCAR STUDY

Fig. 5 (a,b) illustrates the optical microscopy images from the central zone of wear scar of WC-F coating abraded by silica 70 at the lowest and highest applied load, namely 19.6N and 127.5N, respectively. The worn surface reveals the evidence of particle rolling with significant indentation of the surface. In contrast, WC-F coating abraded by alumina 60 experiences particle sliding (grooving) along with small particle rolling across the surface (Fig. 5 (c,d)). Optical microscope analysis of other coatings indicated that silica 70 abrasive results in the particles rolling, while alumina 60 abrasive leads to grooving on the worn surface under all applied loads. Fig. 5 also confirms that the size of indentations, and grooves increase with increasing the applied load.

The plan view SEM images of the wear scars of WC-C coating after abrasion with silica 70 at the lowest and the highest applied loads, namely 19.6N and 127.5N, respectively are demonstrated in Fig. 6 (a,b). Wear scar produced under both loads exhibited removal of cobalt matrix at the higher rate and leaving unprotected carbide particles on the worn surface followed by carbide cracking and pullout, which were more significant under the greater applied load (127.5N). As illustrated in the cross-sectional SEM images under the highest load (Fig. 6c), not only the sub-surface cracking was not significant, but also the carbide grains were standing

proud of the matrix indicating preferential wear of the matrix phase. The carbide cracking combined with void formation is also apparent in Fig. 6c.

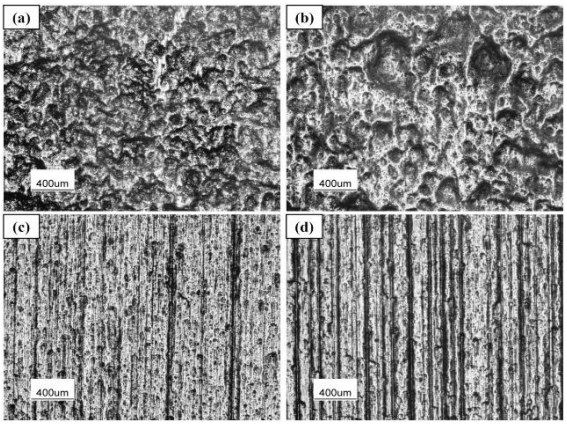

Figure 5. Optical microscopy images of WC-F coating abraded by (a) silica 70 under 19.6N, (b) silica 70 under 127.5N, (c) alumina 60 under 19.6N, and (d) alumina 60 under 127.5N

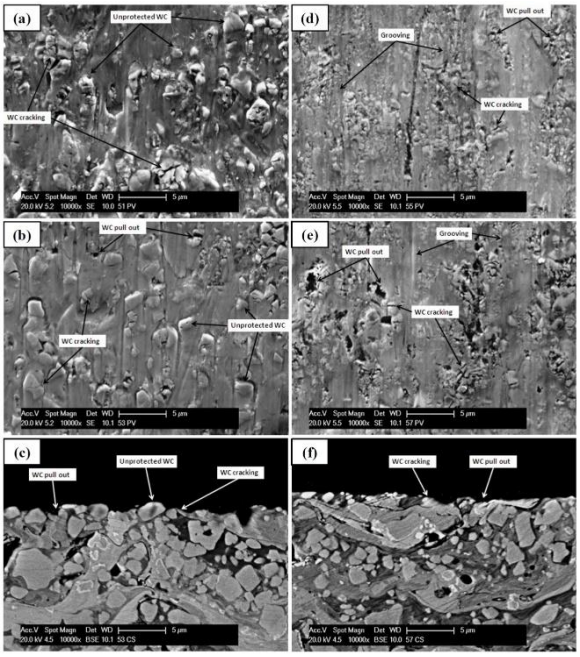

Figure 6. (a,b) Plan view SEM images from wear scar of WC-C coating after abrasion by silica 70 under 19.6 and 127.5N, respectively. (c) Cross-sectional SEM image from wear scar of WC-C coating after abrasion by silica 70 under 127.5N. (d,e) Plan view SEM images from wear scar of WC-C coating after abrasion by alumina 60 under 19.6 and 127.5N, respectively. (f) Cross-sectional SEM image from wear scar of WC-C coating after abrasion by alumina 60 under 127.5N

Fig. 6 (d,e) demonstrates the plan view SEM images of WC-C coating abraded by alumina 60 under 19.6N and 127.5N loads, respectively. Two distinct regions owing low and high density of carbides accompanied by the evidence of grooving, fractured carbide grains, and voids can be detected in Fig. 6 (d,e)due to the carbide pullout. The higher the applied load, the greater the number of voids and cracked carbides appeared on the worn surface. The cross-section of WC-C worn surface abraded by alumina 60 under the highest load (127.5N) (Fig. 6f) exhibits only some small surface pits and no subsurface cracking can be observed.

Fig. 7 (a,b) shows the plan view SEM images from the central zone of the worn surface of WC-F coating abraded by silica 70 at the lowest and the highest loads, namely 19.6N and 127.5N, respectively.

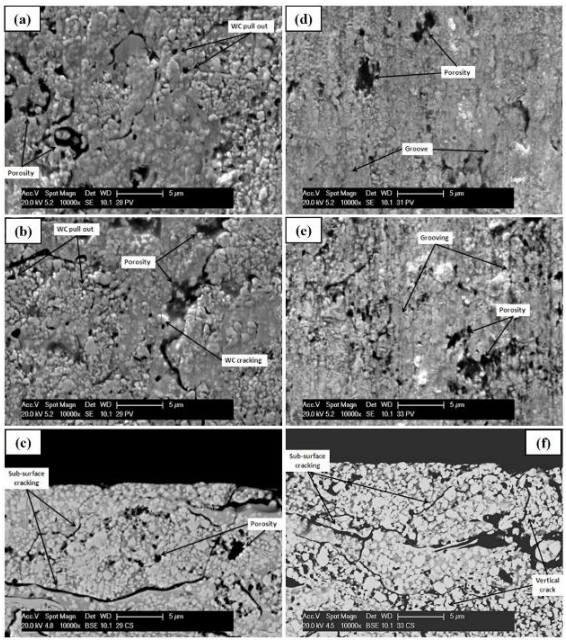

Figure 7. (a,b) Plan view SEM images from wear scar of WC-F coating after abrasion by silica 70 under 19.6 and 127.5N, respectively. (c) Cross-sectional SEM image from wear scar of WC-F coating after abrasion by silica 70 under 127.5N. (d,e) Plan view SEM images from wear scar of WC-F coating after abrasion by alumina 60 under 19.6 and 127.5N, respectively. (f) Cross-sectional SEM image from wear scar of WC-F coating after abrasion by alumina 60 under 127.5N

Many cracks and voids are observed on the wear scar under both applied loads. According to Table 3, the pullout process cannot be easily distinguished because of the high level of porosity in WC-F coating (5.1%). In addition, the metal matrix seems to be exposed to abrasion at a slightly higher rate at which leaves unprotected carbide particles visible in the plan view images (Fig. 7a and b). The cross-sectional SEM image of the worn surface of WC-F coating abraded by silica 70 under the highest applied load (127.5N) is shown in Fig. 7c. The sub-surface crack propagating through the

coating's sub-layers with inherent porosity of the coating is visible in the cross-sectional view of WC-F coating. However, qualitatively good adhesion is apparent between carbide grains and the matrix.

The plan view SEM images of WC-F coating abraded by alumina 60 under 19.6N and 127.5N loads (Fig. 7 (d,e)) display the evidence of grooves and large voids on the worn surface related to either materials loss or presence of open porosities on the coating's surface. Grooving and void formation is more obvious for WC-F coating tested under higher load (127.5N). Besides, the cross-sectional image of the WC-F worn surface (Fig. 7f) reveals a continuous network of cracking along with a wide area of porosity at the sub-surface layer.

Fig 8 (a,b) shows the plan view SEM images from wear scar of WC-N coating abraded by silica 70 under the lowest and highest applied loads, namely 19.6N and 127.5N.

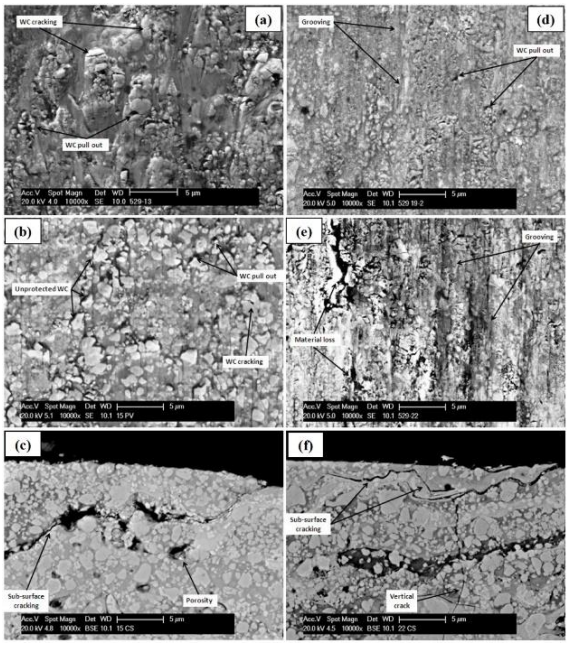

Figure 8. (a,b) Plan view SEM images from wear scar of WCN coating after abrasion by silica 70 under 19.6 and 127.5N, respectively. (c) Cross-sectional SEM image from wear scar of WC-N coating after abrasion by silica 70 under 127.5N. (d,e) Plan view SEM images from wear scar of WC-N coating after abrasion by alumina 60 under 19.6 and 127.5N, respectively. (f) Cross-sectional SEM image from wear scar of WC-N coating after abrasion by alumina 60 under 127.5N

The carbide cracking and pullout are the main abrasive wear mechanisms for the WC-N coating. This mechanism takes place following the faster removal of the metal matrix; hence, the carbide particles are no longer supported by the matrix leading to their pullout and cracking during abrasive wear [16]. The cross-sectional SEM image (Fig. 8c) indicates the good adhesion of carbide particles to the matrix at the subsurface layers of WC-N coating. Besides, sub-surface cracking and porosity are evident in the cross-sectional image of WC-N wear scar.

SEM images of worn surface of WC-N coating abraded by alumina 60 are presented in Fig. 8(d-f). The plan view images under the applied loads of 19.6N (Fig. 8d) and 127.5N (Fig. 8e) show cutting and grooving of both the binder and carbide, with the larger and deeper grooves at the higher load leading to a significant material removal from the worn surface of WC-N coating. The cross-sectional SEM image of the worn surface (Fig. 8f) reveals the evidence of vertical and sub-surface crack propagation through the binder phase.

4. DISCUSSION

4.1. GENERAL OBSERVATIONS

As plotted in Fig. 3, the abrasive wear rate of WC-C, WC-F, and WC-N coatings exhibits an increasing trend with the applied load for both silica 70 and alumina 60 abrasives. However, there is an exception in this trend at 127.5N for several coatings in which the wear rate is unexpectedly reduced. The temperature of both sample and wheel increase during dry sand rubber wheel test depending on various parameters including the abrasive type, sample material, and testing load [28]. The rubber temperature rising as a function of the applied load will result in decreasing its hardness followed by the reduction in wear rate at 127.5N [25].

The abrasive hardness to coating hardness ratio indicated the "hard abrasive wear" by alumina 60 and the "soft abrasive wear" by silica 70 (Fig. 4) indicating significantly lower wear rates with the silica 70 abrasives compared to alumina 60 for all coatings and all examined test conditions (Fig. 3). In addition, low magnification optical microscopy images of the coatings (Fig. 5 (a,c)) indicate particle rolling with significant indentation of the surface caused by silica 70 abrasives, while the alumina 60 resulted in grooves along the direction of abrasive flow. The size of indentations, and grooves increase by increasing the applied load (Fig. 5 (b,d)). The greater hardness and the angular morphology of the alumina 60 compared to the more rounded silica 70 particles (see Fig. 2) can be considered as the main reasons for the significant difference in the wear behavior of the coatings.

Fig. 9 (a,b) displays the wear rate of WC-C, WC-F, and WC-N coatings abraded by silica 70 and alumina 60 as a function of the hardness of the coatings.

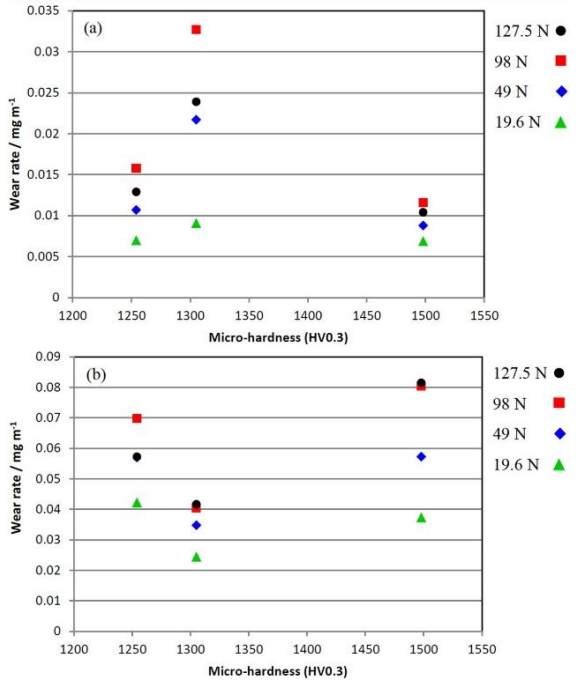

Figure 9. Variation of wear rate as a function of microhardness for WC-C (1305$HV_{0.3}$), WC-F (1498$HV_{0.3}$), and WC-N (1254$HV_{0.3}$) coatings braded by (a) silica 70 and (b) alumina 60

According to plots presented in Fig. 9, the wear rate of the coatings is not necessarily deceased with increasing the hardness of the coatings. For instance, the wear rate of WC-C coating abraded by silica 70 is generally greater than that of WC-N coating despite the higher hardness of the WC-C coating compared to WC-N one (Fig. 9a). Notably, this trend will be reversed by exposing the coatings under abrasion by alumina 60; i.e. WC-N coating with lower hardness suffers from more damage and materials removal as compared to WC-C coating. This can be referred to the complicated mechanism of abrasive wear in thermally sprayed cermet coatings, which make the type of abrasive as a key factor determining the abrasion wear resistance of the coatings.

The WC-C, WC-F, and WC-N coatings can be classified into two groups with distinct characteristics:

Co-group (WC-C) and non-Co-group (WC-F and WC-N). Each group exhibits similar characteristics in the feedstock powder and the resultant coating.

Co-group mostly contains 83wt% WC, while this amount is 85wt% for non-Co-group [7]. Moreover, the carbide shape in the non-Co-group seems to be rounded as compared to the angular carbide grains in the Co-group [7]. Finally, the binder material in the starting powder is a pure metal (Cobalt) for Co-group, whereas there are two complicated alloys (Hastelloy type C for WC-N and Kanthal for WC-F) for non-Co-group as the binder materials [7].

Similar properties of the coatings in each group include:

i) High fracture toughness for Co-group (WC-C: 5.9±0.13MPa.$m^{1/2}$) and low fracture toughness for non-Co-group (WC-F: 3.1±0.23 and WC-N: 2.8±0.27MPa.$m^{1/2}$);

ii) Low porosity for Co-group (WC-C: 1.8%) and high porosity for non-Co-group (WC-F: 5.1% and WC-N: 2.2%);

iii) Higher W_2C and lower amorphous phases in non-Co-group as compared to Co-group [7];

iv) High mean free path for Co-group (WC-C: 0.68µm) and low mean free path for non-Co-group (WC-F: 0.31µm and WC-N: 0.4µm);

v) The high volume fraction of carbide phase for non-Co-group (WC-F: 58% and WC-N: 59%) and lower carbide volume fraction for Co-group (WC-C: 55%).

Based on the abovementioned differences between feedstock powder and coatings of Co-group and non-Co group, the abrasive wear mechanisms of the coatings abraded by silica 70 and alumina 60 can be explained according to the next part of this research.

4.2. ABRASIVE WEAR WITH SILICA 70

The silica 70 abrasives with the lowest hardness compared to other coatings examined (1138±47$HV_{0.3}$) exhibits a rounded morphology with a narrow size distribution. The abrasive hardness (H_a) to the hardness of thr coatings (H_s) ratio is less than 1.2 indicating "soft wear" regime and, as such, particle blunting is most probable during abrasion process resulting in a lower rate of wear under three-body (rolling) abrasion mechanism as compared to the harder abrasive particles. The selective binder phase removal from the near-surface layer is considered as a substantial stage in the wear process of composite materials abraded by soft abrasives [29]. Cyclic indenting contact of abrasive particles during the three-body abrasion process imposes compressive stresses at the surface of the coatings. As a result, the support of the binder is no longer possible for WC particles as parts of the binder are initially extruded out of the surface followed by damage to WC grains located in heavily loaded regions, where the binder phase is abraded. This leads to WC fracture into smaller particles and their gradual pullout from the surface. The situation will be more complicated and the damage will be more severe for WC grains located at the edge of defects such as cracks or areas of surface damage where a greater load is imposed by abrasive particles resulting in the growth of the defects. Consequently, micro-cracks preferentially propagate around the pits and through the W-rich binder phase or along splat boundaries. Elastic-plastic indentation of the abrasive may also form sub-surface cracks into the coating, the propagation of which leads to detachment of fragments of the surface of coatings [30]. The crack initiation caused at the end of an empty space by binder phase removal or carbide grains pullout is observed in

the cross-sectional SEM images of the coatings (e.g., Fig. 7c) indicating crack propagation mostly through the W-rich binder phase or splat boundaries.

The plan view and cross-sectional SEM images are shown in Fig. 6 (a-c). The cobalt matrix removal followed by WC fracture and pullout is the prevalent abrasive wear mechanisms for Co-group (WC-C coating) abraded by silica 70, while limited evidence of micro-grooving and sub-surface cracking were observed indicating the high fracture toughness of Co-group (5.9±0.13MPa.$m^{1/2}$) and high resistance to crack initiation and propagation.

A combination of subsurface cracking, WC pullout, and the fracture was observed for non-Co-group during abrasive wear by silica 70 (see Fig. 7 (a-c) and Fig. 8 (a-c)). The higher density of subsurface cracking could be attributed to the higher porosity and W_2C/WC ratio in non-Co-coatings compared to Co-group leading to lower fracture toughness (WC-F: 3.1±0.23MPa.$m^{1/2}$ and WC-N: 2.8±0.27MPa.$m^{1/2}$) [7].

Non-Co-group abraded by silica 70 particles showed superior wear resistance compared to Co-group.

It has been reported that there is a relationship between abrasion resistance and the mean free path of the binder phase between the carbide grains for the cemented materials. This means that a short mean free path caused by a high volume fraction of fine carbide grains, leads to the highest abrasion resistance [31]. A similar result has been reported for HVOF thermally sprayed WC-based coating abraded by a dry sand rubber wheel test indicating the best abrasion resistance for the coating with the lowest the mean free path [32]. The comparison between mean free path of Co-group (WC-C: 0.68µm) and non-Co-group coatings (WC-F: 0.31µm and WC-N: 0.4µm) reveals significantly lower values for the latter group resulting in their superior abrasion wear resistance.

The abrasive wear behavior of both WC-F and WC-N Coatings (non-Co-group) abraded by silica 70 follows the soft wear regime with low wear rates. It should be noted that the wear rate of WC-N coating is faster than the WC-F one. The greater wear resistance of WC-F could be justified by its lower mean free path and higher hardness as compared to WC-N coating (Table 3).

4.3. ABRASIVE WEAR WITH ALUMINA 60

Alumina 60 abrasive with the highest hardness among the examined coatings (2144±25HV0.3) exhibits an angular morphology with a narrow size range (Fig. 2). The abrasive hardness H_a to the hardness of the coating H_s ratio is more than 1.2 indicating the "hard wear" regime. Abrasive particles cause the plastic deformation mostly by plastic ploughing and cutting accompanied by some local fracture in the more brittle composites under hard abrasive conditions [27].

The worn surface of WC-C, WC-F, and WC-N coatings produced by alumina abrasive (Figs. 6-8 (d-f)) shows the evidence of grooving, pitting, and cutting. The cross-sectional images of the wear scars also indicate a significant sub-surface cracking for WC-F and WC-N coatings while no significant cracking can be detected for WC-C coating, which indicates the high fracture toughness of WC-C coating compared to non-Co coatings. According to the results, two main wear mechanisms can be considered in materials including plastic deformation and fracture. The passage of the hard and sharp abrasives causes the plastic deformation of the surface at the first stage of the abrasion process resulting in the formation of grooves with materials pile up at the groove edges.

A plastic groove forms during embedding and sliding of sharp particles into the surface at the first stage of wear. The penetration extent of the abrasive particles into the surface is different for each coating.

The residual stresses caused by deformation drive the lateral cracks to grow upwards through the coating.

Cross-sectional SEM images of the wear scars of WC-F and WC-N coatings reveal that the subsurface cracks propagate parallel to the top surface of the coatings (Fig. 7f, Fig. 8f). Two types of cracks can be formed due to the low fracture toughness of WC-F and WC-N coatings: Horizontal cracks along the surface and vertical cracks perpendicular to the surface. According to the argument of Stewart et al. [22], formation of vertical cracks caused by the indentation of the abrasive into the coating is the initial stage of the material loss procedure. The vertical cracks run down through the coating and end upon reaching either a region of the W-rich binder phase or a splat boundary. The next step is the crack propagate parallel to the coating surface to reach the surface. In general, this process results in high materials removal in the coatings with low fracture toughness (non-Co-group).

At the second stage, the fatigue of the surface layers and fracture can occur through mechanical deformation leading to the spalling type of failure. A comparison between Co-group and non-Co-group reveals that the fracture mechanism plays more significant role in the wear of the latter owing to its lower fracture toughness that leads to the higher wear rate of WC-F and WC-N coatings compared to WC-C one, as plotted in Fig. 3. In addition, the higher porosity of non-Co-group coatings than Co-group ones can be considered as an important factor in creating more grooves followed by greater material removal.

In summary, WC-C coating exhibited the optimum wear resistance among the coatings abraded by alumina 60 abrasive due to the high fracture toughness and low porosity and protection of WC-C coating against severe cracking and grooving, respectively.

However, the lowest abrasive wear resistance was obtained as for WC-F coating. WC-F is a coating with

high hardness. Nevertheless, the presence of plenty of porosities makes it a coating with low fracture toughness resulting in a large number of grooves at the first stage of the abrasion process and severe cracking at the second stage. Therefore, the wear resistance of WC-F coating is less than other coatings examined, namely WC-C and WC-N.

5. CONCLUSIONS

In this study, the abrasive wear behavior of two advanced WC-based coatings, WC–NiMoCrFeCo (WC-N) and WC–FeCrAl (WC-F), deposited by a Top Gun HVOF system was examined under a soft and hard abrasion regime. The outcomes of investigations were compared to conventional WC-Co (WC-C) coating, as well. The main conclusions can be drawn as follows:

(1) The abrasive wear with silica 70 was located in the "soft abrasion" regime for all coatings, while alumina 60 abrasive imposed a "hard abrasion" regime. Moreover, the wear rate of the coatings abraded by alumina 60 was ~1.2-7.8 times higher than silica 70 abrasive.
(2) Among the coatings tested by silica 70, WC-F exhibited the superior wear resistance owing to its lower mean free path and higher hardness as compared to other coatings.
(3) In the case of Co-group (WC-C) coating abraded by silica 70, the cobalt matrix removal followed by WC fracture and pullout were the prevalent abrasive wear mechanisms. As for non-Co-group coatings (WC-F and WC-N), a combination of subsurface cracking, WC pull-out, and the fracture was operating during abrasive wear by silica 70.
(4) WC-C coating revealed the highest wear resistance relative to other coatings when abraded by alumina 60. This was caused by its high fracture toughness and low porosity, which protect WC-C coating against severe cracking and grooving, respectively.
(5) Examination of the worn surface of WC-C, WC-F, and WC-N coatings after abrasion by alumina 60 showed the evidence of grooving, pitting, and cutting. The cross-sectional images of the wear scars also revealed a significant sub-surface cracking for WC-F and WC-N coatings while no significant cracking was detected for WC-C coating.

6. ACKNOWLEDGEMENTS

The author sincerely appreciate Professors Philip Shipway and Graham McCartney from Department of Mechanical, Materials, and Manufacturing Engineering, The University of Nottingham, UK, for their supervision, advice and encouragement throughout this research.

REFERENCES

1. Yuan, J., Ma, C., Yang, S., Yu, Z., Li, H., "Improving the wear resistance of HVOF sprayed WC-Co coatings by adding submicron-sized WC particles at the splats' interfaces", ***Surface and Coatings Technology***, Vol. 285, (2016), 17-23.
2. Trpčevská, J., Ganev, N., Żórawski, W., Jakubeczyova, D., Briančin, J., "Effect of powder particle size on the structure of HVOF WC-Co sprayed coatings", ***Powder Metallurgy Progress***, Vol. 9, No. 1, (2009), 42-48.
3. Stewart, D. A., Shipway, P. H., McCartney, D. G., "Microstructural evolution in thermally sprayed WC-Co coatings: comparison between nanocomposite and conventional starting powders", ***Acta Materialia***, Vol. 48, No. 7, (2000), 1593-1604.
4. Mateen, A., Saha, G. C., Khan, T. I., Khalid, F. A., "Tribological behaviour of HVOF sprayed near-nanostructured and microstructured WC-17wt.% Co coatings", ***Surface and Coatings Technology***, Vol. 206, No. 6, (2011), 1077-1084.
5. Gong, T., Yao, P., Zuo, X., Zhang, Z., Xiao, Y., Zhao, L., Zhou, H., Deng, M., Wang, Q., Zhong, A., "Influence of WC carbide particle size on the microstructure and abrasive wear behavior of WC–10Co–4Cr coatings for aircraft landing gear", ***Wear***, Vol. 362-363, (2016), 135-145.
6. Jafari, M., Enayati, M. H., Salehi, M., Nahvi, S. M., Park, C. G., "Microstructural and mechanical characterizations of a novel HVOF-sprayed WC-Co coating deposited from electroless Ni–P coated WC-12Co powders", ***Materials Science and Engineering: A***, Vol. 578, (2013), 46–53.
7. Nahvi, S. M., Jafari, M., "Microstructural and mechanical properties of advanced HVOF-sprayed WC-based cermet coatings", ***Surface and Coatings Technology,*** Vol. 286, (2016), 95-102.
8. Berger, L. M., "Applications of hardmetals as thermal spray coatings", ***International Journal of Refractory Metals and Hard Materials***, Vol. 49, (2015), 350-364.
9. Park, S. Y., Kim, M. C., Park, C. G., "Mechanical properties and microstructure evolution of the nano WC–Co coatings fabricated by detonation gun spraying with post heat treatment", ***Materials Science and Engineering: A***, Vol. 449-451, (2007), 894-897.
10. Myalska, H., Moskal, G., Szymański, K., "Microstructure and properties of WC-Co coatings, modified by sub-microcrystalline carbides, obtained by different methods of high velocity spray processes", ***Surface and Coatings Technology***, Vol. 260, (2014), 303-309.
11. Qiao, Y., Fischer, T. E., Dent, A., "The effects of fuel chemistry and feedstock powder structure on the mechanical and tribological properties of HVOF thermal-sprayed WC-Co coatings with very fine structures", ***Surface and Coatings Technology***, Vol. 172, No. 1, (2003), 24-41.
12. Picas, J. A., Punset, M., Baile, M. T., Martín, E., Forn, A., "Effect of oxygen/fuel ratio on the in-flight particle parameters and properties of HVOF WC-CoCr coatings", ***Surface and Coatings Technology***, Vol. 205, (2011), S364-S368.
13. Sobolev, V. V., Guilemany, J. M., Nutting, J., "High velocity oxy-fuel spraying: Theory, structure-property relationships and applications", London: Maney Publishing, (2004).
14. De Villiers Lovelock, H. L., "Powder/processing/structure relationships in WC-Co thermal spray coatings: A review of the

published literature", ***Journal of Thermal Spray Technology***, Vol. 7, No. 3, (1998), 357-373.

15. Yuan, J., Zhu, Y., Zheng, X., Ruan, Q., Ji, H., "Improvement in tribological properties of atmospheric plasma-sprayed WC-Co coating followed by Cu electrochemical impregnation", ***Applied Surface Science***, Vol. 255, No. 18, (2009), 7959-7965.
16. Jafari, M., Enayati, M. H., Salehi, M., Nahvi, S. M., Hosseini, S. N., Park, C. G., "Influence of nickel-coated nanostructured WC-Co powders on microstructural and tribological properties of HVOF coatings", ***Journal of Thermal Spray Technology***, Vol. 23, No. 8, (2014), 1456-1469.
17. Baik, K. H., Kim, J. H., Seong, B. G., "Improvements in hardness and wear resistance of thermally sprayed WC-Co nanocomposite coatings", ***Materials Science and Engineering: A***, Vol. 449-451, (2007), 846-849.
18. Saha, G. C., Khan, T. I., "The corrosion and wear performance of microcrystalline WC-10Co-4Cr and near-nanocrystalline WC-17Co high velocity oxy-fuel sprayed coatings on steel substrate", ***Metallurgical and Materials Transactions A***, Vol. 41, No. 11, (2010), 3000–3009.
19. Aristizabal, M., Rodriguez, N., Ibarreta, F., Martinez, R., Sanchez, J. M., "Liquid phase sintering and oxidation resistance of WC–Ni–Co–Cr cemented carbides", ***International Journal of Refractory Metals and Hard Materials***, Vol. 28, No. 4, (2010), 516–522.
20. Birks, N., Meier, G. H., Pettit, F. S., "Introduction to the High-Temperature Oxidation of Metals", 2nd ed., Cambridge University Press: UK, (2006).
21. Nerz, J., Kushner, B., Rotolico, A., "Microstructural Evaluation of Tungsten Carbide-Cobalt Coatings", ***Journal of Thermal Spray Technology***, Vol. 1, No. 2, (1992), 147-152.
22. Stewart, D. A., Shipway, P. H., Mccartney, D. G., "Abrasive wear behaviour of conventional and nanocomposite HVOF-sprayed WC–Co coatings", ***Wear***, Vol. 225–229, (1999), 789–798.
23. Dent, A. H., Depalo, S., Sampath, S., "Examination of the wear properties of HVOF sprayed nanostructured and conventional WC–Co cermets with different binder phase contents", ***Journal of Thermal Spray Technology***, Vol. 11, No. 4, (2002), 551–558.
24. Khan, T. I., Saha, G., Glenesk, L. B., "Nanostructured composite coatings for oil sands applications", ***Surface Engineering***, Vol. 26, No7, (2010), 540-545.
25. Stevenson, A. N. J., Hutchings, I. M., "Development of the dry sand rubber wheel abrasion test", ***Wear***, Vol. 195, No. 1-2, (1996), 232-240.
26. ASTM G 65-00, "Standard Test Method for Measuring Abrasion Using the Dry Sand/Rubber Wheel Apparatus", ASTM International West Conshohocken, PA., (2000), 256-267.
27. Hutchings, I. M., Shipway, P. H., "Tribology: friction and wear engineering materials", Oxford: Butterworth-Heinemann, (2017), 273.
28. Nahvi, S. M., Shipway, P. H., McCartney, D. G., "Particle motion and modes of wear in the dry sand-rubber wheel abrasion test", ***Wear***, Vol. 267, No. 11, (2009), 2083-2091.
29. Blombery, R. I., Perrot, C. M., Robinson, P. M., "Abrasive wear of tungsten carbide-cobalt composites. I. Wear mechanisms", ***Materials Science and Engineering,*** Vol. 13, No. 2, (1974), 93-100.
30. Chen, H., Xu, C., Zhou, Q., Hutchings, I. M., Shipway, P. H., Liu, J., "Micro-scale abrasive wear behaviour of HVOF sprayed and laser-remelted conventional and nanostructured WC-Co coatings", ***Wear***, Vol. 258, No. 1-4, (2005), 333-338.
31. Larsen-Basse, J., "Effect of composition, microstructure, and service conditions on the wear of cemented carbides", ***The Journal of the Minerals, Metals & Materials Society (JOM)***, Vol. 35, No. 11, (1983), 35-42.
32. Kumari, K., Anand, K., Bellacci, M., Giannozzi, M., "Effect of microstructure on abrasive wear behaviour of thermally sprayed WC-10Co-4Cr coatings", ***Wear***, Vol. 268, No. 11-12, (2010), 1309-1319.